Zwitterionic Functionalizable Scaffolds with Gyroid Pore Architecture for Tissue Engineering

Nina Yu. Kostina, Sébastien Blanquer, Ognen Pop-georgievski, Khosrow Rahimi, Barbara Dittrich, Anita Höcherl, Jiří Michálek, Dirk Grijpma, Cesar Rodriguez-emmenegger

Zwitterionic Functionalizable Scaffolds with Gyroid Pore Architecture for Tissue Engineering

Nina Yu. Kostina, Sébastien Blanquer, Ognen Pop-georgievski, Khosrow Rahimi, Barbara Dittrich, Anita Höcherl, Jiří Michálek, Dirk Grijpma, Cesar Rodriguez-emmenegger

FULL PAPERS

Q1 xxxx

Zwitterionic biodegradable hydrogels with gyroid pore architecture are fabricated by stereolithography. The addition of zwitterionic carboxybetaine to the polymerization resins endow hydrogels with improved swelling and functional groups. Hydrogels show suppression of fouling from protein solutions while could be selectively functionalized by preactivation of the carboxylate groups.

Macromolecular Bioscience
www.mbs-journal.de

Zwitterionic Functionalizable Scaffolds with Gyroid Pore Architecture for Tissue Engineering

Nina Yu Kostina, Sebastien Blanquer, Ognen Pop-Georgievski, Khosrow Rahimi, Barbara Dittrich, Anita Höcherl, Jiří Michálek, Dirk W. Grijpma, and Cesar Rodriguez-Emmenegger*

Stereolithography-assisted fabrication of hydrogels of carboxybetaine methacrylamide and a α,ω-methacrylate poly(D,L-lactide-*block*-ethylene glycol-*block*-D,L-lactide) telechelic triblock macromer is presented. This technique allows printing complex structures with gyroid interconnected porosity possessing extremely high specific area.

Hydrogels are characterized by infrared spectroscopy, X-ray photoelectron spectroscopy, and confocal laser scanning microscopy. The copolymerization with zwitterionic comonomer leads hydrogels with high equilibrium water content, up to 700% while maintaining mechanical robustness. The introduction of carboxybetaine yields excellent resistance to nonspecific protein adsorption while providing a facile way for specific biofunctionalization with a model protein, fluorescein isothiocyanate labeled bovine serum albumin. The homogeneous protein immobilization across the hydrogel pores prove the accessibility to the innermost pore volumes.

The remarkably low protein adsorption combined with the interconnected nature of the porosity allowing fast diffusion of nutrient and waste product and the mimicry of bone trabecular, makes the hydrogels presented here highly attractive for tissue engineering.

1. Introduction

The primary goal of tissue engineering is to provide a biological surrogate to regenerate damaged or malfunctioning tissues.[1–4] The reconstruction of most of the tissues requires a template guiding the organization of cells. Thus, scaffolding was introduced to tissue engineering to provide active support and signals for cells' growth, migration, and new tissue formation.[1,5,6] Cell migration is controlled by a complex set of mechanisms that are affected not only by extra- and intracellular signaling but also by surrounding extracellular environment.[7] Scaffold microstructure, such as porosity, pore size and shape, specific surface area, interconnectivity, has been shown to significantly affect cell adhesion, growth, and differentiation. Such scaffolds are used for in vivo regeneration of various tissues, such as skin, cartilage, bone, and peripheral nerves.[7–11] Access to nutrients is a cornerstone for cell growth and survival. Thus, interconnectivity of pores are essential for unrestricted fluid flow through the pore space and to ensure diffusion of nutrients, metabolic waste products, cytokines, and paracrine factors through the scaffold.[12]

Conventional strategies for scaffold preparation rely on the covalent or physical cross-linking of polymers to create a matrix.[13,14] However, the size of such mesh (nanometer scale) is well below cell size (larger than several μm) which makes it impossible for cells to crawl and colonize the whole matrix. To circumvent this, several strategies to create macroporosity (micrometer scale) have been introduced, including solvent casting/particulate leaching, fibril networking, and phase separation.[15–20] However, the use

Dr. N. Y. Kostina, Dr. K. Rahimi, Dr. B. Dittrich, Dr. C. Rodriguez-Emmenegger
DWI—Leibniz Institute for Interactive Materials and Institute of Technical and Macromolecular Chemistry
RWTH Aachen University
Forckenbeckstraße 50, 52074 Aachen, Germany
E-mail: rodriguez@dwi.rwth-aachen.de
Dr. S. Blanquer
Institute Charles Gerhardt Montpellier
CNRS—University of Montpellier—ENSCM
34095 Montpellier, Cedex 5, France
The ORCID identification number(s) for the author(s) of this article can be found under https://doi.org/10.1002/mabi.201800403.
Dr. O. Pop-Georgievski, Dr. A. Höcherl, Dr. J. Michálek
Institute of Macromolecular Chemistry
Academy of Sciences of the Czech Republic
v.v.i. Heyrovsky sq. 2, Prague 162 06, Czech Republic
Prof. D. W. Grijpma
Department of Biomaterials Science and Technology Group
Technical Medical Centre
University of Twente
P.O. Box 217, 7500 AE Enschede, The Netherlands
Prof. D. W. Grijpma
W.J. Kolff Institute
Department of Biomedical Engineering
University Medical Center Groningen
University of Groningen
Antonius Deusinglaan 1, 9713 AV Groningen, The Netherlands

DOI: 10.1002/mabi.201800403

of these techniques is limited due to the difficulty of having a perfect control over the internal pore architecture resulting in structures with irregular pore sizes and often poor pore interconnectivity.[21] Alternatively, the advances in additive manufacturing significantly improved the production of scaffolds with precise geometry and internal morphology.[22–24] Among them, stereolithography is one of the most developed computer-aided rapid prototyping technique.[12,23,24] It exploits the 3D-controlled solidification of liquid-based resins by photopolymerization. The structure is polymerized in a layer-by-layer manner which allows the fabrication of complex 3D scaffolds with precise external and internal architecture with the highest accuracy.[12,24–26] In particular gyroid-type structures can be written with very high precision. Gyroid structures of various length scales are ubiquitous in nature from membranes of organelles to milk particles.[27] The triply periodic gyroid-structure has unique properties such as the highest surface area available and perfectly interconnected porosity.[28]

For tissue engineering not only is the architecture of the pores important but also the chemistry of the exposed surface. The polymers used for stereolithography play an important role in the scaffold fabrication. Photo-cross-linkable polymer solutions—resins—are often based on the mixture of (meth) acrylate-functionalized oligomers, photoinitiators, and a nonvolatile solvent and the viscosity of the mixture is carefully optimized.[23,29] However, the surfaces generated from such polymers are rapidly fouled by proteins from the tissue culture media causing an abundance of negative side effects.

To induce specific cell attachment, the surface of the scaffold should be decorated with biological cues, such as peptides, or proteins interacting with integrin receptors of the cell.[30,31] However, it becomes very challenging for real application when the decorated scaffold comes in contact with biological fluids, such as blood plasma or other bodily fluids. This induces nonspecific protein adsorption, that is, protein fouling, leading to irreversible changes in the properties of the material.[32,33] This protein fouling interferes with the signaling mechanisms by masking the biological elements immobilized at the surface and by creating a film of proteins which supports the nonspecific adhesion of cells.[32–42] Thus the fabrication of materials able to resist nonspecific protein adsorption is essential.[42] Although several strategies to modify the surface of 2D materials with coatings resistant to fouling have been achieved, the problem of protein fouling for 3D scaffolds used in tissue engineering is generally neglected.[33,35,37,43] Only a few attempts were made in the preparation of 3D scaffolds able to resist protein fouling and most of them were based on poly(ethylene glycol) (PEG).[34,38,39,44,45] However, recently Riedel et al. proved that their contact with real biological media led to fouling regardless of the type of polymer architecture.[33,37,46,47] None of the PEG-based surface modifications could resist the fouling from human blood plasma. The deposits on the best antifouling brushes consisted of apolipoprotein A-I, apolipoprotein B-100, complement C3, complement C4-A, complement C4-B, Fbg, histidine-rich glycoprotein, the Ig mu chain C region, and HSA. These proteins were ubiquitous in all of the deposits on PEG-based surfaces suggesting some degree of biospecificity, thus alternative to PEG should be sought.[46]

Previously, it has been shown that polymers based on zwitterionic carboxybetaines are able to completely suppress fouling from complex biological media, such as saliva, urine, cerebrospinal liquid, blood plasma, and whole blood.[35,37,48,49] Recently, our group has introduced antifouling hydrogels consisted of zwitterionic carboxybetaines.[38,39] These hydrogels were prepared by copolymerization of 2-hydroxyethyl methacrylate with carboxybetaine acrylamide or methacrylamide and showed a dramatic decrease of protein fouling from complex biological fluids, such as fetal bovine serum and undiluted human blood plasma.[38,39] Additionally, the carboxybetaine moieties endowed hydrogels with available functional groups which can be utilized for the immobilization of specific biological molecules.[38,39,50]

Herein we introduce a novel type of zwitterionic antifouling hydrogels with precise gyroid pore architecture by employing the unique properties of nonfouling zwitterionic poly(carboxybetaine)s and a technique for fabrication of scaffolds with designed architecture, such as stereolithography. The hydrogels were prepared by copolymerization of zwitterionic carboxybetaine methacrylamide (CBMAA) and a macromer α,ω-methacrylate poly(D,L-lactide-*block*-ethylene glycol-*block*-D,L-lactide) telechelic triblock copolymer (MA-PDLLA-PEG-PDLLA-MA) as cross-linker. The poly(D,L-lactide) (PDLLA) block is introduced for biodegradability, while the poly(ethylene glycol) (PEG) block confers hydrophilicity. Both ends of the macromer are functionalized with methacrylate groups to allow the copolymerization with the zwitterionic comonomer. The successful copolymerization was confirmed by infrared spectroscopy with attenuated total reflectance (FTIR-ATR) and X-ray photoelectron spectroscopy (XPS). The copolymerization of MA-PDLLA-PEG-PDLLA-MA macromer with CBMAA monomer led to hydrogels with unique properties. On one hand, these hydrogels showed antifouling character—the absence of nonspecific interaction with proteins, but on the other hand, their available carboxyl groups can be utilized for specific immobilization of bioactive compounds. In order to demonstrate this, the hydrogels were functionalized with fluorescently labeled bovine serum albumin (BSA), which was selected as a model protein.

2. Experimental Section

2.1. Materials

3,6-Dimethyl-1,4-dioxane-2,5-dione (D,L-lactide), α,ω-dihydroxy poly(ethylene glycol) (α,ω-dihydroxy PEG) ($\bar{M}_n$ = 4000 g mol^{-1}), tin(II) 2-ethylhexanoate ($Sn(Oct)_2$) (92.5–100%), methacrylic anhydride (MAAH) (94%), triethylamine (TEA) (≥99%), *N*-[3-(dimethylamino)propyl]methacrylamide (99%), *N*-hydroxysulfosuccinimide sodium salt (sulfoNHS) (≥98%), *N*-(3-dimethylaminopropyl)-*N*′-ethylcarbodiimide hydrochloride (EDC), BSA–fluorescein isothiocyanate conjugate (BSA-FITC) were purchased from Sigma-Aldrich. β-Propiolactone was purchased from Serva electrophoresis GmbH. Lucirin TPO-L (ethyl-2,4,6-trimethylbenzoyl phenylphosphinate) was acquired from BASF (Germany). Phenol red was supplied by Riedel de Haën.

Isopropanol, dichloromethane, diethyl ether, chloroform, tetrahydrofuran, and methanol were purchased from Lachner.

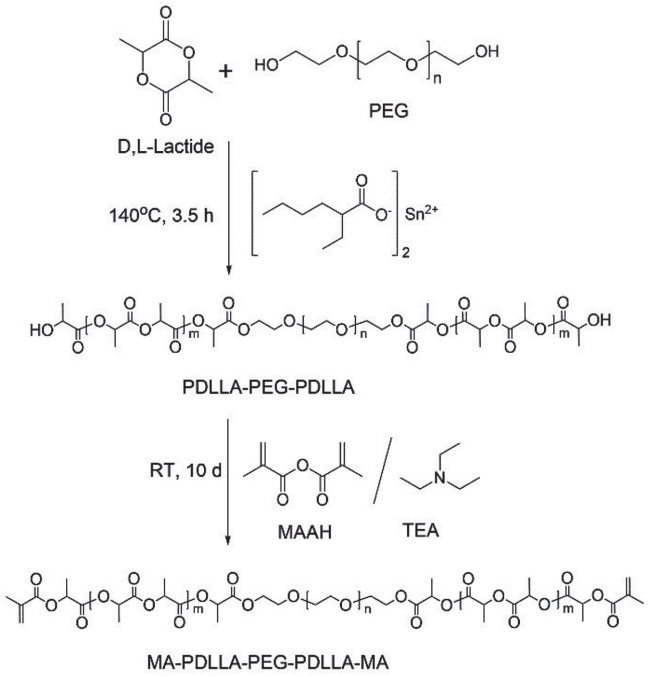

Scheme 1. Synthesis of PDLLA-PEG-PDLLA oligomer and MA-PDLLA-PEG-PDLLA-MA macromer.

Tetrahydrofuran (anhydrous THF, ≥99.9%), diethyl ether (anhydrous, ≥99.7), and phosphate-buffered saline (PBS, pH 7.4) were purchased from Sigma-Aldrich.

2.2. Synthesis of MA-PDLLA-PEG-PDLLA-MA Macromer

The synthesis of MA-PDLLA-PEG-PDLLA-MA macromer (**Scheme 1**) was performed in a two-step reaction. In the first step D,L-lactide was polymerized from the hydroxyl end groups of PEG. This was followed by conjugation with methacrylate groups to generate a telechelic macromer.

2.2.1. Synthesis of PDLLA-PEG-PDLLA

PDLLA-PEG-PDLLA was synthesized by a ring-opening polymerization of D,L-lactide initiated from the terminal hydroxyl groups of α,ω-dihydroxy PEG catalyzed by $Sn(Oct)_2$ (Scheme 1).[51] The targeted molecular weight of the oligomers was between 4500 and 5000 g mol^{-1}. Firstly, 300 g (75 mmol) of α,ω-dihydroxy PEG was molten and dried in a three-necked flask, under vacuum and magnetic stirring, at 120 °C for 10 h. Then 86.5 g (0.6 mol) of D,L-lactide and 0.6 g (1.5 mmol) $Sn(Oct)_2$ was added under argon atmosphere. The molar ratio of D,L-lactide/$Sn(Oct)_2$ was 400/1. The reaction was carried out for 3.5 h at 140 °C. Afterwards, isopropanol was added to the reaction mixture. This alcohol is a good solvent for the monomer and catalyst while the polymer precipitates and can be recovered by filtration with copious washing.

2.2.2. Synthesis of MA-PDLLA-PEG-PDLLA-MA Macromer

The oligomer was functionalized with methacrylate groups (MA) by acylation of the terminal hydroxyl groups of the PDLLA-PEG-PDLLA oligomer with MAAH (Scheme 1). Solutions of PDLLA-PEG-PDLLA (C = 0.25 g mL^{-1}) and MAAH (C = 0.2 g mL^{-1}) in dry DCM were prepared in separate flasks and purged with argon for 20 min. Then TEA (18 mL) was injected into the solution of oligomer under argon. The solution of MAAH was added to the solution of oligomer and TEA by dropping funnel. The reaction was allowed to proceed for 10 days with continuous stirring. The formed MA-PDLLA-PEG-PDLLA-MA was precipitated into dry diethyl ether and purified by dissolving in chloroform and reprecipitating into diethyl ether.[52]

2.3. Synthesis of Carboxybetaine Methacrylamide (3-Methacryloylamino-propyl)-(2-carboxy-ethyl)-dimethyl-ammonium)

CBMAA was synthesized by a modified procedure reported earlier (**Scheme 2**).[53,54] (The synthetic procedure is described in the ESI).

2.4. Optimization of the Stereolithography Resin Composition and Building of Hydrogel Structures

Resins of different compositions were prepared (**Table 1**). The MA-PDLLA-PEG-PDLLA-MA macromer, CBMMA monomer (Table 1) and phenol red dye were dissolved in Milli-Q water to give solution 1. Lucirin TPO-L (visible light photo-initiator) was dissolved in DMSO to give solution 2. Solution 1 and 2 were combined and stirred at room temperature until a clear liquid resin was formed. The final resin composition was: 30 wt% of the mixture of macromer and monomer, 4.95 wt% of Lucirin TPO-L, 0.05 wt% of phenol red, 50 wt% of water and 15 wt% of DMSO. The weight ratio of CBMAA to MA-PDLLA-PEG-PDLLA-MA was varied from 0 to 20%.

Hydrogels were prepared using Perfactory Mini Multilens stereolithography apparatus (Envision-Tec, Germany) equipped

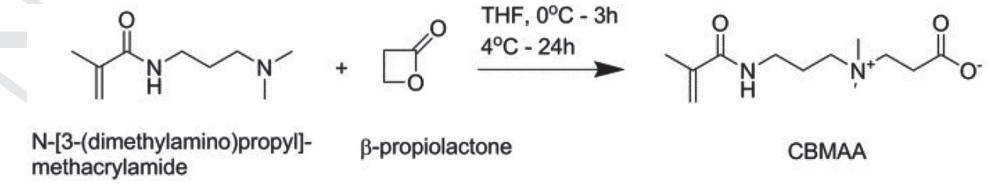

Scheme 2. Synthesis of CBMAA.

Table 1. Composition of formulations of hydrogels with different weight ratio of macromer to monomer.

Hydrogels abbreviation	MA-PDLLA-PEG-PDLLA-MA / CBMAA [wt%]
0% CBMAA	100 / 0
10% CBMAA	90 / 10
20% CBMAA	80 / 20

with a digital micro-mirror device that enables projections of 1280 × 1024 pixels, each measuring 32 × 32 μm^2. Hydrogels with gyroid-type porosity were prepared by the sequential illumination, polymerization, and cross-linking of layers of the resin. For this, the resin was exposed to a pixel pattern of blue light (wavelength 400–550 nm, peak intensity at 440 nm) while the z-position of the platform was moved step-wise (25 μm) to allow the formation of a 3D structure. The gyroid pore structures of hydrogels were designed using Rhinoceros 3D (McNeel Europe) and K3DSurf computer software as described elsewhere.[55]

The fabrication of the hydrogel structures was carried out by exposing the photopolymerizable resin to light intensities of 10 mW cm^{-2}. The curing time for a 25-μm-thick layer was evaluated from the working curves obtained for each type of resin formulation—40 s for 0%CBMAA, 54 s for 10%CBMAA and 57 s for 20%CBMAA. After photo-polymerization, the obtained structures were washed with acetone (1 day), water (2 days), acetone (1 day) to remove any non-cross-linked compounds. The samples were dried at room temperature for 1 day under atmospheric pressure and subsequently in vacuum until constant weight. Flat nonporous samples were also produced for XPS and FTIR analysis.

2.5. Functionalization of Hydrogels with BSA-FITC

BSA-FITC was covalently immobilized on the pores of the gyroids structures using EDC/sulfoNHS coupling. Hydrogels of each formulation (0% CBMAA, 10% CBMAA, and 20% CBMAA) were swollen in water and then placed in individual vials containing a solution of EDC (C = 0.522 M) and sulfoNHS (C = 0.115 M) in water. This solution creates active esters of the CBMAA monomers which can be attacked by amine groups of proteins for their covalent immobilization. The samples were shaken for 2 h at room temperature. Subsequently, hydrogels with activated carboxyl groups were washed three times with water, allowing at least 20 min for each wash. Then the activated hydrogels were placed to PBS for 1 h. After incubation, each sample was placed into 4 mL of fresh PBS solution and 2 mL of stock-solution of BSA-FITC (C = 3.33 mg mL^{-1}) was added. The reaction was allowed to proceed in the dark for 2 h at room temperature and then for 12 h at 4 °C. Finally, the hydrogels were thoroughly washed with copious amounts of PBS and stored in this buffer overnight. Confocal imaging was performed after an incubation period of at least one day.

In order to prove the absence of nonspecific adsorption of BSA-FITC on the hydrogels, blank experiments were performed. Hydrogels of each formulation were swollen in PBS solution. Then the swollen hydrogels were transferred to vials containing 4 mL of fresh PBS to which 2 mL of stock-solution of BSA-FITC (C = 3.33 mg mL^{-1}) was added. The incubation time, washing procedures, and imaging were performed as above.

2.6. Characterization of Oligomer, Macromer, and Hydrogels

2.6.1. Proton Nuclear Magnetic Resonance

^{1}H NMR spectra of reaction products were recorded on Bruker DPX 300 and utilized to determine conversion of D,L-lactide, chemical structure, molecular weight of PDLLA-PEG-PDLLA and degree of functionalization with MAAH. $CDCl_3$ was used as a solvent.

2.6.2. Fourier Transform Infrared Spectroscopy with Attenuated Total Reflectance

The chemical structure of synthesized PDLL-PEG-PDLLA oligomer and MA-PDLLA-PEG-PDLLA-MA-co-CBMAA hydrogels were characterized by FTIR-ATR. Spectra were recorded using an FTIR Thermo Nicolet Nexus 670 spectrometer equipped with a Specac Golden Gate attachment and a diamond reflection prism.

2.6.3. X-Ray Photoelectron Spectroscopy

The chemical composition of the hydrogels was investigated by XPS. The measurements were carried out with a K-Alpha+ spectrometer (Thermo Fisher Scientific). The samples were analyzed using a micro-focused, monochromated Al Kα X-ray source (400 μm spot size). The kinetic energy of the electrons was measured using a 180° hemispherical energy analyzer operated in the constant analyzer energy mode (CAE) at 200 eV and 50 eV pass energy for survey and high resolution spectra. Data acquisition and processing were performed using Thermo Advantage software. The XPS spectra were fitted with one or more Voigt profiles (binding energy (BE) uncertainty: ± 0.2 eV). The analyzer transmission function, Scofield sensitivity factors,[56] and effective attenuation lengths (EALs) for photoelectrons were applied for quantification. EALs were calculated using the standard TPP-2M formalism.[57] All spectra were referenced to the C 1s peak of hydrocarbons at 285.0 eV BE controlled by means of the well-known photoelectron peaks of PET and metallic Cu, Ag, and Au.

2.6.4. Swelling Properties of Hydrogels

The equilibrium water content (EWC) of porous hydrogels was determined gravimetrically. Five samples of each composition of hydrogels were immersed in deionized water and allowed to swell until constant mass (5 days) and the mass of the swollen samples was determined (m_s). Subsequently, the samples were dried under vacuum at room temperature to constant weight

and the mass of dry hydrogels (m_d) was determined. The EWC was calculated as:

$$EWC\,(\%) = \frac{m_s - m_d}{m_d} * 100\% \quad (1)$$

2.6.5. Laser Scanning Confocal Microscopy

Hydrogels with immobilized BSA-FITC were visualized using the Olympus multiphoton LSCM with the FV10-ASW viewer software (Olympus, Japan). Images were recorded using a 4×-air objective and a 488 nm laser for excitation of FITC; emission was detected at 500–530 nm. 3D reconstructed images were obtained by stacking 20 LSCM *xy*-scans at 0.5 µm intervals using the ImageJ software.

3. Results and Discussion

In this study, we report the preparation of a novel type of zwitterionic functionalizable hydrogels with gyroid pore architecture. These hydrogels were prepared by copolymerization of macromer (MA-PDLLA-PEG-PDLLA-MA) with the zwitterionic monomer (CBMAA) utilizing stereolithography.

3.1. Synthesis of PDLLA-PEG-PDLLA Oligomer and MA-PDLLA-PEG-PDLLA-MA Macromer

The PDLLA-PEG-PDLLA oligomer was synthesized by ring-opening polymerization of D,L-lactide, initiated by the hydroxyl terminal groups of the PEG chain (Scheme 1). The conversion of D,L-lactide was determined from ^{1}HNMR spectra of the reaction mixture (Figure S1, Supporting Information). When the lactide cycle is opened, protons of the methyl groups present in D,L-lactide are shifted from δ 1.64–1.61 to δ 1.60–1.37 ppm. The conversion was calculated as the ratio of the integral of the shifted peaks (δ 1.60–1.37 ppm) to the sum of integrals of shifted peaks and peaks of residual D,L-lactide (δ 1.64–1.61 ppm) (Equation S1, Supporting Information) and was equal to 93%.

A prominent band at 1750 cm^{-1} in the FTIR-ATR spectrum of PDLLA-PEG-PDLLA assigned to ester carbonyl confirms the successful polymerization of D,L-lactide (Figure S2, Supporting Information). On the ^{1}HNMR spectrum a peak at δ 4.13–4.42 ppm, corresponding to methylene protons of the PEG connected to PDLLA could be discerned proving the structure of PDLLA-PEG-PDLLA (Figures S1 and Figure S3, Supporting Information). The degree of polymerization of D,L-lactide (m) was calculated by comparing the integrals corresponding to protons of methylene groups of PEG (δ 3.20–3.90 ppm in Figure S3, Supporting Information) and protons of methyl lactyl units (δ 1.37–1.60 ppm in Figure S3), considering the average degree of polymerization of PEG is DP_n = 91 (Equation S2, Supporting Information). The NMR-degrees of polymerization were used to calculated the number average molecular weight of PDLLA-PEG-PDLLA oligomer $\bar{M}_n$ = 5250 g mol^{-1}.

The hydroxyl end groups of the synthesized PDLLA-PEG-PDLLA oligomer were acylated with MAAH to obtain the MA-PDLLA-PEG-PDLLA-MA macromer (Scheme 1). The incorporation of methacrylate groups to PDLLA-PEG-PDLLA was confirmed by the appearance of three signals in the ^{1}HNMR spectrum of the macromer: at δ 6.14, 5.58, and 1.90 ppm, corresponding to the = CH_2 and –CH_3 of the methacrylate groups (Figure S4, Supporting Information). The complete disappearance of the signals of terminal hydroxyls in PDLLA-PEG-PDLLA (δ 2.83) indicates that all end-groups contain a methacrylate. This was further confirmed by comparing the integrals of protons of the methacrylate group (δ 6.14 and 5.57 ppm) with those of PEG (δ 3.40–3.80 ppm) considering the number-average degree of polymerization (DP_n = 91).[52]

3.2. Preparation and Characterization of Hydrogels

A precise control over the cure depth of resin is necessary for fabrication of structures by stereolithography. In order to achieve well defined structures it is necessary to tune the cross-linking depth. The polymerization is initiated from an inverted platform that moves upward to generate each layer. Upon irradiation, only part of the resin, which is at focal plane of the laser beam, is cross-linked. The cross-linked volume must be thick enough so that when the platform moves upwards (away from the focal plane) the next cross-linked volume will be grown from the previously formed structure. On the other hand if the depth of cross-linking is too deep then the structure blurs and the pores close.[24,58,59] The cure depth is determined by the light energy to which the resin is exposed. This energy can be adjusted by the illumination time or by regulating the light intensity. The relationship between the effective cure depth of the resin and the light irradiation dose can be expressed using Equation (2) derived from the Beer–Lambert law:

$$C_d = D_p \cdot \ln\left(\frac{E}{E_c}\right) \quad (2)$$

where C_d is cure depth, E is the energy of the light to which the resin has been exposed, E_c is the critical energy for curing, which represents the minimum energy level required for cross-linking of the resin, and D_p is the penetration depth.

Experimentally, an optimal exposure time is determined by constructing the working curve, a plot of the C_d versus the natural logarithm of the energy ln(E). From the intercept and slope of the working curve, the critical energy E_c and penetration depth of light into resin D_p can be determined. The critical exposure and penetration depth are very important parameters and must be evaluated for each resin formulation before the scaffold fabrication to prevent the failure of interlayer bonding or inaccuracies in the architecture.[52,55]

Resins based on MA-PDLLA-PEG-PDLLA-MA with different weight ratio of CBMAA were prepared (Table 1). A 0.05 wt% of phenol red dye was added to each formulation to restrict the penetration depth of the light and gain better control over the layer thickness.[60] The working curves for all resin compositions were obtained by varying the energy of the light exposed

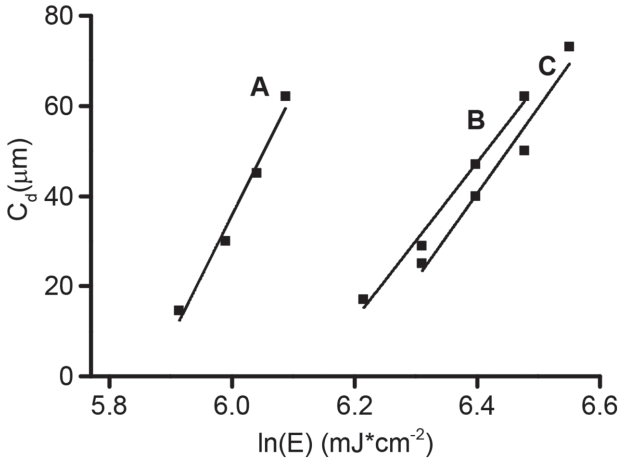

Figure 1. Stereolithography working curves for A) 0% CBMAA, B) 10% CBMAA, and C) 20% CBMAA resins.

at the resin surface (E) and measuring the resulting cure depths (C_d) of the resins (**Figure 1**). The required curing times for a 25-μm-thick layer at a light intensity equal to 10 mW cm^{-2} were calculated to be 40 s, 54 s, and 57 s for 0% , 10% , and 20% CBMAA resins respectively.

Nonporous films and hydrogels with gyroid pore architecture were fabricated by stereolithogaphy utilizing resins containing different amount of zwitterionic comonomer CBMAA. All hydrogel structures were soft and highly flexible, their shape and structure precisely matched their design. The chemical structure of the hydrogels was confirmed by FTIR-ATR (**Figure 2**). The increase in the amount of zwitterionic comonomer was evidenced by the concomitant increase in the intensity of amide bands at 1650 cm^{-1} and 1535 cm^{-1}, and the carboxyl band at 1600 cm^{-1} arising from the CBMAA added to the resin formulation.

In addition, the chemical composition of hydrogels was further evidenced using XPS. **Figure 3** reports the high resolution core level C 1s and N 1s regions of spectra of the

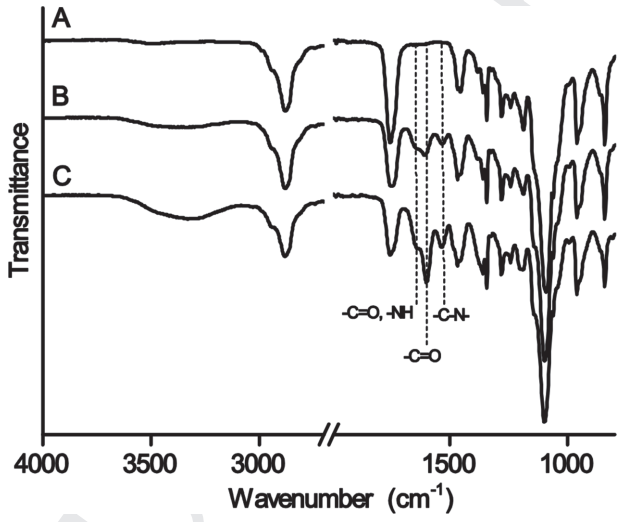

Figure 2. FTIR-ATR spectra of hydrogels prepared from different formulations of resin: A) 0% CBMAA, B) 10% CBMAA, and C) 20% CBMAA.

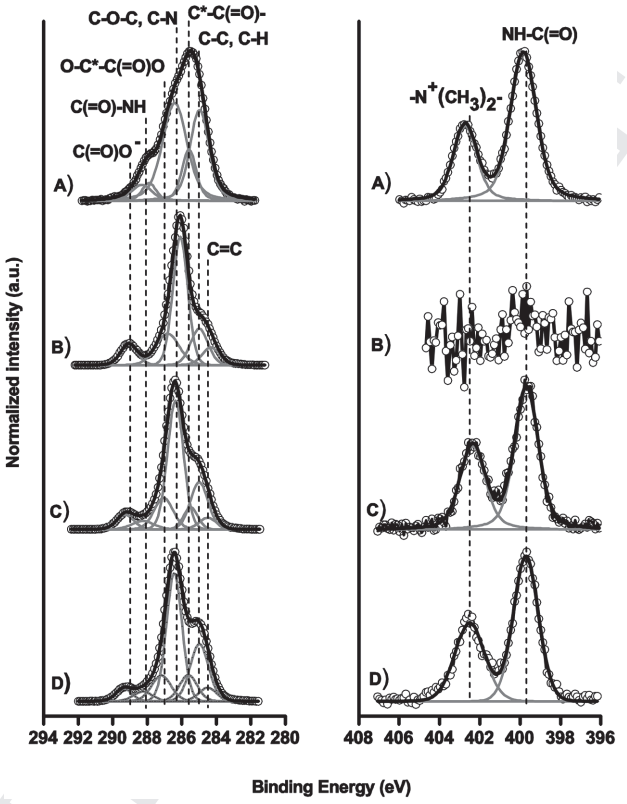

Figure 3. High resolution C 1s (left) and N 1s (right) XPS spectra of A) pure poly(CBMAA), B) 0%CBMAA, C) 10%CBMAA, and D) 20%CBMAA dry hydrogels.

bulk poly(CBMAA) material and 0%CBMAA, 10%CBMAA, and 20%CBMAA hydrogels. The C 1s spectrum of poly(CBMAA) bulk material is characterized by a C−C contribution at 285.0 eV, which is accompanied by contributions at 285.6 ± 0.1 eV, 286.2 ± 0.2 eV, 287.9 ± 0.1 eV, and 288.3 ± 0.1 eV arising from the secondary chemical shift,, that is, the effect of the amide group on the tertiary carbon atom in the CH$_3$−C*−C(=O)−NH structure, the C−N$^+$ moieties, the amide group C(=O)−NH and the carboxylic (O−C=O) group. The N 1s spectrum of poly(CBMAA) is characterized by contributions at about 399.5 ± 0.1 eV and 402.5 ± 0.1 eV of amides and charged quaternary ammonium groups, respectively. The 0%CBMAA hydrogel shows the characteristic contributions for the lactide and ethylene oxide monomers as well as the methacrylate groups that did not react during the photo-curing reaction. The contributions centered at 284.5 ± 0.1 eV, 285.0 eV, 286.3 ± 0.2 eV, 287.0 ± 0.2 eV, and 289.0 ± 0.5 eV arise from the C=C, C−C, C−O−C, O−C*−C(=O)O, and ester O−C=O group, respectively. The N 1s spectrum of 0%CBMAA completely lacks nitrogen (amides and charged quaternary ammonium groups) contributions.

The incorporation of CBMAA monomer units into the MA-PDLLA-PEG-PDLLA-MA structure is clearly observed in the high resolution C 1s and N 1s spectra of the 10%CBMAA and 20%CBMAA hydrogels. The presence of CBMAA can be verified by the rise of the contributions of C−C at 285.0 eV, CH$_3$−C*−C(=O)−NH at 285.6 ± 0.1 eV, the C—N$^+$ moieties

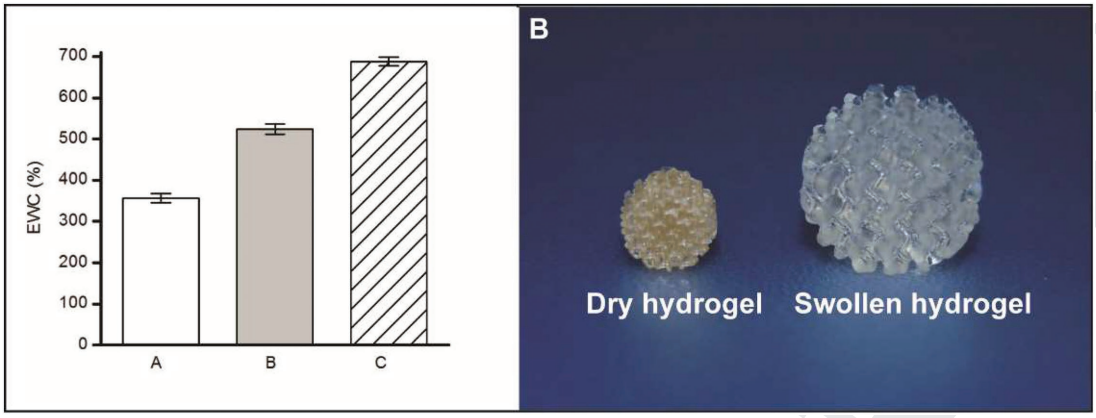

Figure 4. The equilibrium water content (EWC) of hydrogels A) 0% CBMAA, B) 10% CBMAA, and C) 20% CBMAA, defined as the ratio between the mass of absorbed water after reaching the equilibrium and the mass of dried hydrogels (left). The photograph shows dry and swollen hydrogel of 10% CBMAA (right).

(which strongly overlap with the O—C*—C(=O)O contributions of PDLLA at 286.3 ± 0.2 eV) and the C(=O)—NH group at 288.1 ± 0.2 eV within the C 1s spectra, as well as the occurrence of contributions arising from amide at 399.7 ± 0.1 eV and charged quaternary ammonium groups at 402.5 ± 0.1 eV in the high resolution N 1s spectra. The increase of CBMAA in the polymerization feed from 10 to 20% lead to an increase of the nitrogen content from 1.3 at.% to 2.8 at.%.

The swelling behavior and water uptake capability are essential parameters of scaffolds for tissue engineering. Highly wetted scaffolds provide a good environment for cell growth and proliferation. However, water content of all natural tissues differs depending on the tissue function. Thus, it is of high importance to be able to tune the water content in order to match the properties of targeted tissue. The copolymerization of macromer MA-PDLLA-PEG-PDLLA-MA with zwitterionic comonomer CBMAA can enable tuning the swelling properties of the hydrogels.[38,39] As expected, an increase in the amount of CBMAA in the polymerization resin lead to an increase of EWC of hydrogels (**Figure 4**). A 50% increase in swelling was observed with the addition of only 10% of CBMAA to the polymerization feed. A further increment in the CBMAA concentration to 20% led to hydrogel with remarkable water content reaching the value of 700%.

3.3. Protein Immobilization on Hydrogel Pores

A widely used approach to induce specific cell adhesion is to immobilize biomolecules, such as peptides or proteins, on the surface of the scaffold to interact with integrin receptors of the cell. To immobilize the bioactive compounds, the material of the scaffold must possess available functional groups while preventing any nonspecific interactions that can occur at the interface between the biological medium and the surface of the scaffold. To achieve this, CBMAA was introduced as a comonomer for the preparation of hydrogels. It was hypothesized that the copolymerization of the macromer with CBMAA will provide not only available carboxylic groups for the biofunctionalization but also will ensure the resistance to nonspecific interaction with proteins.

The pores of the hydrogels were functionalized with a fluorescently-labeled model protein, BSA-FITC. For this, carboxylate groups of the carboxybetaine monomers were activated with EDC/sulfoNHS in water, followed by incubation with a protein solution in PBS buffer (**Figure 5**D–F). To prove the specificity of the binding we performed control experiments by incubating with BSA-FITC for 14 h without any previous activation with EDC/sulfoNHS. No fluorescence was observed on nonactivated hydrogels during the scanning of all hydrogels (0%, 10%, and 20%CBMAA) with a 488 nm laser for excitation of FITC proving the absence of nonspecific albumin adsorption on the hydrogels (Figure 5A–C).

As expected, no BSA immobilization was observed on the hydrogel without any addition of CBMAA (0%CBMAA) (Figure 5D), due to the lack of functional groups on hydrogels. On the other hand, hydrogels containing 10% and 20% of CBMAA were successfully biofunctionalized with BSA-FITC as presented in Figure 5E,F. These hydrogels show strong fluorescence emission stemming from BSA-FITC. ImageJ software was used to measure the mean average intensity of the pixels in the fluorescent area in order to analyze the difference in the fluorescence intensity in hydrogels containing 10 and 20%CBMAA. The fluorescence intensity of hydrogels containing 10%CBMAA was 22.8 ± 4.3 a.u., while that of hydrogels with 20%CBMAA was 33.4 ± 5.0 a.u.; emitting almost 32% more light. The larger fluorescent signal is well in line with the higher amount of functionalizable carboxylate groups. Figure 5G depicts the 3D reconstruction of 20 confocal scans of 10%CBMAA hydrogel after biofunctionalization showing that the pores were homogeneously modified all across the structure.

4. Conclusions

Stereolithography was utilized to fabricate non-fouling hydrogels with a precisely designed interconnected porosity. The hydrogels were prepared by copolymerization of macromer MA-PDLLA-PEG-PDLLA-MA and CBMAA. The addition of CBMAA comonomer endowed the hydrogels with an increase in EWC, reaching an unprecedented level of 700% for 20%CBMAA. The

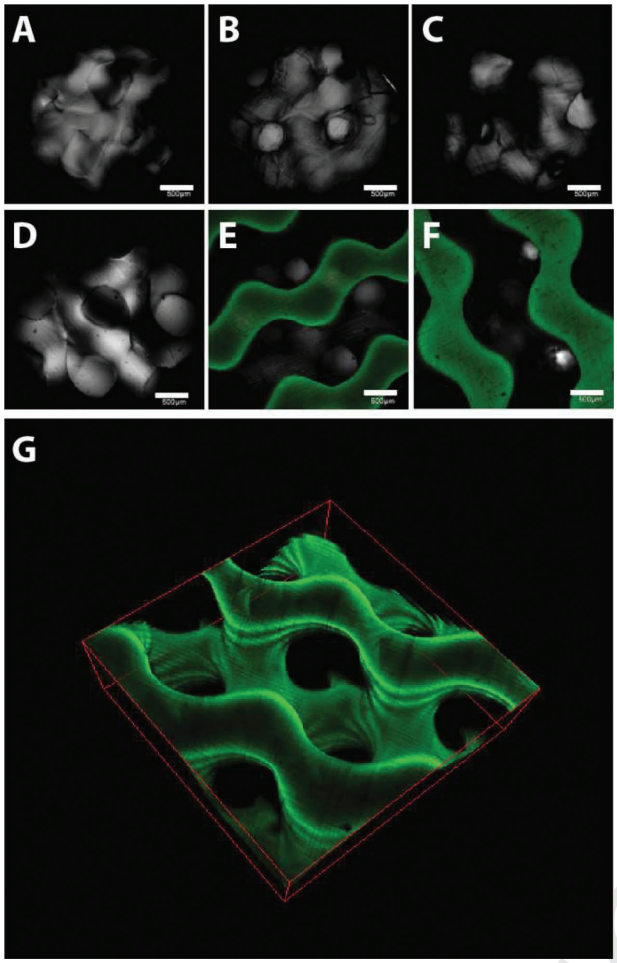

Figure 5. Biofunctionalization of gyroid hydrogels with BSA-FITC observed by confocal laser microscopy. The contact of BSA-FITC with non-activated hydrogels shows no fluorescence (A–C for 0, 10 and 20% CBMAA hydrogels respectively). D–F are confocal images of hydrogels with 0, 10 and 20% of CBMAA preactivated with EDC/sulfoNHS. The strong fluorescence in E and F proves the successful biofunctionalization. Image G represents the 3D reconstruction of 20 confocal *xy* scans of 10% CBMAA hydrogels with immobilized BSA-FITC.

CBMAA monomers endowed the hydrogels with antifouling properties while biofunctionalizable. The open interconnected porosity allowed the modification of the surface of the pores with proteins as evidenced by LSCM.

The hydrogels described here represent a novel and highly promising scaffold for tissue engineering. The shape and pore architecture of hydrogels can be precisely designed and implemented by stereolithography. The combination of oligomer based on hydrophilic (PEG) and degradable (PDLLA) segments and a zwitterionic comonomer endows these hydrogels the tunable swelling properties, antifouling character and available functional groups for the immobilization of bioactive compound.

Supporting Information

Supporting Information is available from the Wiley Online Library or from the author.

Acknowledgements

N.Y.K. acknowledges the Alexander von Humboldt Foundation, O.P.G. acknowledges the support from the Grant Agency of the Czech Republic (GACR) under Contract No. 16–02702S, J.M. acknowledges the support from the Grant Agency of the Czech Republic (GACR) under Contract No. 16–04863S, A.H. acknowledges the Ministry of Education, Youth and Sports of the Czech Republic (grant POLYMAT #LO1507).

Conflict of Interest

The authors declare no conflict of interest.

Keywords

gyroid pore structure, hydrogels, stereolithography, zwitterionic

Received: October 18, 2018
Revised: December 17, 2018
Published online:

[1] B. D. Ratner, A. S. Hoffman, F. J. Schoen, J. E. Lemons, *Biomaterials Science: An Introduction to Materials in Medicine, Second Edition*, Elsevier Academic Press **2004**.
[2] R. Langer, J. P. Vacanti, *Science* **1993**, *260*, 920.
[3] R. Langer, *Mol. Ther.* **2000**, *1*, 12.
[4] R. Pirraco, R. Reis, *Stem Cell Rev. Rep.* **2015**, *11*, 373.
[5] N. Huebsch, D. J. Mooney, *Nature* **2009**, *462*, 426.
[6] N. A. Peppas, J. Z. Hilt, A. Khademhosseini, R. Langer, *Adv. Mater.* **2006**, *18*, 1345.
[7] B. A. C. Harley, H.-D. Kim, M. H. Zaman, I. V. Yannas, D. A. Lauffenburger, L. J. Gibson, *Biophys. J.* **2008**, *95*, 4013.
[8] V. Karageorgiou, D. Kaplan, *Biomaterials* **2005**, *26*, 5474.
[9] F. J. O'Brien, B. A. Harley, I. V. Yannas, L. J. Gibson, *Biomaterials* **2005**, *26*, 433.
[10] Q. Zhang, H. Lu, N. Kawazoe, G. Chen, *Acta Biomater.* **2014**, *10*, 2005.
[11] M. Madaghiele, L. Salvatore, A. Sannino, in *Biomedical Foams for Tissue Engineering Applications*, P. A. Netti, Ed., Woodhead Publishing **2014**, p. 101.
[12] F. P. Melchels, A. M. Barradas, C. A. van Blitterswijk, J. de Boer, J. Feijen, D. W. Grijpma, *Acta Biomater.* **2010**, *6*, 4208.
[13] N. Gjorevski, N. Sachs, A. Manfrin, S. Giger, M. E. Bragina, P. Ordóñez-Morán, H. Clevers, M. P. Lutolf, *Nature* **2016**, *539*, 560.
[14] A. S. Hoffman, *Adv. Drug Delivery Rev.* **2012**, *64*, 18.
[15] J. C. Ashworth, S. M. Best, R. E. Cameron, *Mater. Technol.* **2014**, *29*, 281.
[16] M. V. Baker, D. H. Brown, Y. S. Casadio, T. V. Chirila, *Polymer* **2009**, *50*, 5918.
[17] Š. Kubinová, D. Horák, N. Kozubenko, V. Vaněček, V. Proks, J. Price, G. Cocks, E. Syková, *Biomaterials* **2010**, *31*, 5966.
[18] H. Studenovská, M. Šlouf, F. Rypáček, *J. Mater. Sci.: Mater. Med.* **2007**, *19*, 615.
[19] N. Annabi, J. W. Nichol, X. Zhong, C. Ji, S. Koshy, A. Khademhosseini, F. Dehghani, *Tissue Eng., Part B* **2010**, *16*, 371.
[20] J. G. Torres-Rendon, T. Femmer, L. De Laporte, T. Tigges, K. Rahimi, F. Gremse, S. Zafarnia, W. Lederle, S. Ifuku, M. Wessling, J. G. Hardy, A. Walther, *Adv. Mater.* **2015**, *27*, 2989.
[21] G. Antonio, R. Teresa, D. S. Roberto, A. Luigi, *J. Appl. Biomater. Biomech.* **2009**, *7*, 141.

[22] M. A. Przeradzka, B. van Bochove, T. C. Bor, D. W. Grijpma, *Polym. Adv. Technol.* **2017**, *28*, 1212.
[23] B. van Bochove, G. Hannink, P. Buma, D. W. Grijpma, *Macromol. Biosci.* **2016**, *16*, 1853.
[24] F. P. Melchels, J. Feijen, D. W. Grijpma, *Biomaterials* **2010**, *31*, 6121.
[25] S. A. Skoog, P. L. Goering, R. J. Narayan, *J. Mater. Sci.: Mater. Med.* **2014**, *25*, 845.
[26] S. B. G. Blanquer, M. Werner, M. Hannula, S. Sharifi, G. P. R. Lajoinie, D. Eglin, J. Hyttinen, A. A. Poot, D. W. Grijpma, *Biofabrication* **2017**, *9*, 025001.
[27] S. Salentinig, H. Amenitsch, A. Yaghmur, *ACS Omega* **2017**, *2*, 1441.
[28] N. Vargas-Alfredo, A. Dorronsoro, A. L. Cortajarena, J. Rodriguez-Hernandez, *ACS Appl. Mater. Interfaces* **2017**, *9*, 37454.
[29] S. Schuller-Ravoo, J. Feijen, D. W. Grijpma, *Macromol. Biosci.* **2011**.
[30] B. Wehrle-Haller, *Curr. Opin. Cell Biol.* **2012**, *24*, 116.
[31] R. W. Sands, D. J. Mooney, *Curr. Opin. Biotechnol.* **2007**, *18*, 448.
[32] C. Blaszykowski, S. Sheikh, M. Thompson, *Chem. Soc. Rev.* **2012**, *41*, 5599.
[33] C. Rodriguez Emmenegger, E. Brynda, T. Riedel, Z. Sedlakova, M. Houska, A. B. Alles, *Langmuir* **2009**, *25*, 6328.
[34] N. Y. Kostina, O. Pop-Georgievski, M. Bachmann, N. Neykova, M. Bruns, J. Michálek, M. Bastmeyer, C. Rodriguez-Emmenegger, *Macromol. Biosci.* **2016**, *16*, 83.
[35] C. Rodriguez-Emmenegger, E. Brynda, T. Riedel, M. Houska, V. Subr, A. B. Alles, E. Hasan, J. E. Gautrot, W. T. Huck, *Macromol. Rapid Commun.* **2011**, *32*, 952.
[36] C. Rodriguez-Emmenegger, A. Jäger, E. Jäger, P. Stepanek, A. B. Alles, S. S. Guterres, A. R. Pohlmann, E. Brynda, *Colloids Surf., B* **2011**, *83*, 376.
[37] C. Rodriguez-Emmenegger, M. Houska, A. B. Alles, E. Brynda, *Macromol. Biosci.* **2012**, *12*, 1413.
[38] N. Y. Kostina, C. Rodriguez-Emmenegger, M. Houska, E. Brynda, J. Michálek, *Biomacromolecules* **2012**, *13*, 4164.
[39] N. Y. Kostina, S. Sharifi, A. D. Pereira, J. Michalek, D. W. Grijpma, C. Rodriguez-Emmenegger, *J. Mater. Chem. B* **2013**, *1*, 5644.
[40] C. Blaszykowski, S. Sheikh, M. Thompson, *Trends Biotechnol.* **2014**, *32*, 61.
[41] A. de los Santos Pereira, S. Sheikh, C. Blaszykowski, O. Pop-Georgievski, K. Fedorov, M. Thompson, C. Rodriguez-Emmenegger, *Biomacromolecules* **2016**, *17*, 1179.
[42] M. Thompson, C. Blaszykowski, S. Sheikh, C. Rodriguez-Emmenegger, A. De los Santos Pereira, *Biological Fluid-Surface Interactions in Detection and Medical Devices*, The Royal Society of Chemistry, Cambridge, UK **2016**.
[43] C. Rodriguez-Emmenegger, S. Janel, A. de los Santos Pereira, M. Bruns, F. Lafont, *Polym. Chem.* **2015**, *6*, 5740.
[44] C.-C. Lin, K. Anseth, *Pharm. Res.* **2009**, *26*, 631.
[45] J. L. Drury, D. J. Mooney, *Biomaterials* **2003**, *24*, 4337.
[46] T. Riedel, Z. Riedelová-Reicheltová, P. Májek, C. Rodriguez-Emmenegger, M. Houska, J. E. Dyr, E. Brynda, *Langmuir* **2013**, *29*, 3388.
[47] C. Rodriguez-Emmenegger, O. Kylián, M. Houska, E. Brynda, A. Artemenko, J. Kousal, A. B. Alles, H. Biederman, *Biomacromolecules* **2011**, *12*, 1058.
[48] F. Surman, T. Riedel, M. Bruns, N. Y. Kostina, Z. Sedláková, C. Rodriguez-Emmenegger, *Macromol. Biosci.* **2015**, *15*, 636.
[49] H. Vaisocherová, W. Yang, Z. Zhang, Z. Cao, G. Cheng, M. Piliarik, J. Homola, S. Jiang, *Anal. Chem.* **2008**, *80*, 7894.
[50] F. Obstals, M. Vorobii, T. Riedel, A. de Los Santos Pereira, M. Bruns, S. Singh, C. Rodriguez-Emmenegger, *Macromol. Biosci.*1700359, **2018**, *18*.
[51] D. Cohn, A. Hotovely-Salomon, *Polymer* **2005**, *46*, 2068.
[52] T. M. Seck, F. P. Melchels, J. Feijen, D. W. Grijpma, *J. Controlled Release* **2010**, *148*, 34.
[53] C. Rodriguez-Emmenegger, B. V. Schmidt, Z. Sedlakova, V. Subr, A. B. Alles, E. Brynda, C. Barner-Kowollik, *Macromol. Rapid Commun.* **2011**, *32*, 958.
[54] J. G. Weers, J. F. Rathman, F. U. Axe, C. A. Crichlow, L. D. Foland, D. R. Scheuing, R. J. Wiersema, A. G. Zielske, *Langmuir* **1991**, *7*, 854.
[55] F. P. W. Melchels, J. Feijen, D. W. Grijpma, *Biomaterials* **2009**, *30*, 3801.
[56] J. H. Scofield, *J. Electron Spectrosc. Relat. Phenom.* **1976**, *8*, 129.
[57] S. Tanuma, C. J. Powell, D. R. Penn, *Surf. Interface Anal.* **1994**, *21*, 165.
[58] S. C. Ligon, R. Liska, J. Stampfl, M. Gurr, R. Mulhaupt, *Chem. Rev.* **2017**, *117*, 10212.
[59] T. S. Srivatsan, T. S. Sudarshan, *Additive Manufacturing: Innovations, Advances, and Applications*, CRC Press Taylor&Francis Group **2015**.
[60] A. Ronca, L. Ambrosio, D. W. Grijpma, *Acta Biomater.* **2013**, *9*, 5989.

Macromolecular Bioscience

Reprint Order Form 2018

Editorial Office:
Wiley-VCH Verlag
Boschstraße 12, 69469 Weinheim
Germany

Tel.: +49 (0) 6201 – 606 – 581
Fax: +49 (0) 6201 – 606 – 510
Email: macromol@wiley-vch.de

Short DOI: mabi. _____

Please send me and bill me for

no. of **Reprints** via ☐ airmail (+ 25 Euro)
☐ surface mail

Please send me and bill me for a

☐ **high-resolution PDF file** (330 Euro).

My Email address:

_____

Please note: It is not permitted to present the PDF file on the internet or on company homepages.

Information regarding VAT

Please note that from German sales tax point of view, the charge for **Reprints, Issues or Posters** is considered as **"supply of goods"** and therefore, in general, such delivery is a subject to German sales tax. However, this regulation has no impact on customers located outside of the European Union. Deliveries to customers outside the Community are automatically tax-exempt. Deliveries within the Community to institutional customers outside of Germany are exempted from the German tax (VAT) only if the customer provides the supplier with his/her VAT number. The VAT number (value added tax identification number) is a tax registration number used in the countries of the European Union to identify corporate entities doing business there. It starts with a country code (e.g. FR for France, GB for Great Britain) and follows by numbers.

VAT no.: _____

(Institutes / companies in EU countries only)

Purchase Order No.: _____

Delivery address / Invoice address:

Name of recipient, University, Institute, Street name and Street number, Postal Code, Country

_____

_____

_____

_____

_____

_____

_____

Date and Signature: _____

Credit Card Payment (optional) -You will receive an invoice.

VISA, MasterCard, AMERICAN EXPRESS

Please use the Credit Card Token Generator located at the website below to create a token for secure payment. The token will be used instead of your credit card number.

Credit Card Token Generator:
https://www.wiley-vch.de/editorial_production/index.php

Please transfer your token number to the space below.

Credit Card Token Number

Price list for reprints (The prices include mailing and handling charges. All Wiley-VCH prices are exclusive of VAT)

No. of pages	Price (in Euro) for orders of 50 copies	100 copies	150 copies	200 copies	300 copies	500 copies
1-4	345	395	425	445	548	752
5-8	490	573	608	636	784	1077
9-12	640	739	786	824	1016	1396
13-16	780	900	958	1004	1237	1701
17-20	930	1070	1138	1196	1489	2022
for every additional 4 pages	147	169	175	188	231	315

Wiley-VCH Verlag GmbH & Co. KGaA; Location of the Company: Weinheim, Germany;
Trade Register: Mannheim, HRB 432833, Chairman of the Board: Mark Allin
General Partner: John Wiley & Sons GmbH, Location: Weinheim, Germany
Trade Register Mannheim, HRB 432296,
Managing Directors: Sabine Steinbach, Dr. Guido F. Herrmann

WILEY-VCH